Preliminary Assessment of Non-Lagrangian Methods for Penetration Simulation

Leonard E. Schwer
Schwer Engineering & Consulting Services
6122 Aaron Court
Windsor CA 95492
707-837-0559
Len@Schwer.net

Abstract

Lagrangian, Eulerian, and Smooth Particle Hydrodynamics formulations are applied to the simulation of a rigid fragment impacting a concrete panel. An effort is made to keep much of the computational model constant across the simulations. All three methods are shown to be appropriate for this class of ballistic impact simulation. The results and conclusions are preliminary, but the paper serves as an introduction to these alternative forms of penetration analysis.

Introduction

Simulation of penetration events requires a numerical technique that allows one body (penetrator) to pass through another (target). Traditionally these simulations have been performed using either an Eulerian approach, i.e. a non-deformable (fixed) mesh with material advecting among the cells, or using a Lagrangian approach, i.e. a deformable mesh, with large mesh deformations. The chief criticism of the Eulerian approach has been that the shape of the penetrating body, usually a steel projectile, becomes 'fuzzy' as the penetration simulation proceeds due to the mixing of advected materials in the fixed Eulerian cells. Lagrangian methods require some form of augmentation to minimize or eliminate large mesh distortions. Two often used augmentations for Lagrangian penetration simulations are the so called 'pilot hole' technique and mesh erosion. In the pilot hole technique elements are removed, a priori, from the target mesh along the penetrator trajectory; this technique works (surprisingly) well for normal impacts where the trajectory is know a priori. The mesh erosion technique removes distorted elements from the simulation, along the penetrator trajectory, based upon a user supplied criteria; no general guidance exists for selecting such criteria, i.e. they are ad hoc.

The focus of the present work is to perform a preliminary assessment of a relatively new class of numerical methods, referred to as meshfree methods, that offer analysts an alternate analytical technique for simulating this class of ballistic problems, without a priori trajectory knowledge, nor resorting to ad hoc measures. This preliminary assessment is made through the comparison of techniques, as applied to a slightly idealized ballistic impact experiment. The techniques compared are Lagrangian with and without erosion, an Eulerian technique that preserves the projectile shape, and the meshfree method known as Smooth Particle Hydrodynamics. This is admittedly an apples-to-oranges-to-pears comparison, but an effort has been made to minimize the numerous ancillary aspects of the different simulations and focus on the capability of the techniques. To minimize unintended differences in the simulations, the following three key modeling aspects remain constant:

1. Only one software package (code) is used,
2. The same constitutive model is used,
3. The majority of the mesh remains the same.

Also, the simulations were performed using 20% of the internally computed stable time increment, which varied depending upon the analysis formulation. The 20% scale factor was chosen because the fragment's initial impact speed is about 30% of the wave speed in the concrete, so the initial incremental strain-rates are fairly large.

Even with these considerable constraints on the simulations, it is obvious that the results are subject to the user's knowledge and skills in applying the various analysis techniques to the fragment impact simulation. Thus the reader should not assess the merits of these techniques on the provided 'answers,' but should instead focus on the relative merits of each technique and their applicability to specific simulations of interest to the reader.

Problem Description

The impact of fragments on concrete walls is of interest to those designing protective structures. In the present work only one of the single fragment impact is consider, using an idealized of a concrete wall to simplify the numerical modeling. The modeled concrete panel is square with a span-to-thickness ratio of 3.33. The concrete has a nominal unconfined compressive strength of 46 MPa (6.6 ksi). The fragment is a 90 grain (5.8 grams) steel cylinder with a length-to-diameter ratio of 1.268 that is assumed to impact the center of the panel end-on at 3505 ft/sec (1068 m/sec).

Generic Model Description

The concrete panel (target), see Figure 1, is modeled as one quarter of a circular cylinder, i.e. two symmetry planes are used, with a diameter of 508 mm and a thickness of 152 mm. No reinforcement is included in the panel model. The model is constructed using several concentric cylinders. The outer two cylinders, i.e. Zones 1 & 2 shown in Figure 1, have a fairly coarse mesh and are prescribed to be an elastic material. The inner two concentric cylinders, and hexahedra core, i.e. Zones 3, 4, 5, and 6, use a more refined mesh. The two cylinder-mesh refinements, i.e. between Zones 3 & 4, are connected through a tied surface-to-surface constraint. A non-linear material is prescribed for the inner most cylinder and hexahedra core, i.e. Zones 4, 5 & 6. An elastic material was prescribed for the remaining concentric cylinder, i.e. Zone 3. The hexahedra core, i.e. square cross-section through the thickness of the target, is further subdivided into two zones, half-way through the panel thickness. The lower portion of the hexahedra core, i.e. Zone 5 furthest from the fragment, will remain unchanged, as will the remainder of the mesh with the following exception. The upper zone, Zone 6 nearest the fragment, will be replaced with an Eulerian mesh, or a particle mesh, for the non-Lagrangian simulations. The standard elements used in the simulations are 8 node solids with a single integration point; here referred to as the Lagrangian portion of the mesh.

The fragment is modeled as a rigid body, with the density of steel, and prescribed initial velocity. The fragment interacts with the target through a contact interface; the definition of this contact interface changes, depending on the analysis technique used to represent the target.

The concrete is modeled using a two surface plasticity model, where the shear failure surface and pressure-volume strain (compaction) surface are independent; this is sometimes referred to as a 'flat cap' model. In LS-DYNA [2] this constitutive model is known as Material Model 16, or the Pseudo-TENSOR model. The shear failure surface parameters were obtained by calibrating the model to available material characterization data, as shown in Figure 2. The pressure-volume strain response is a generic (default) calibration obtained from the model by specifying the concrete density (2.26×10^{-4} g/mm) and unconfined compressive strength (46 MPa), and is shown in Figure 3. A tensile strength of 4 MPa is also a generic (default) calibration based on the concrete's unconfined compression strength. The elastic parameters are the shear modulus of 14.47 GPa and a Poisson's ratio of 0.116.

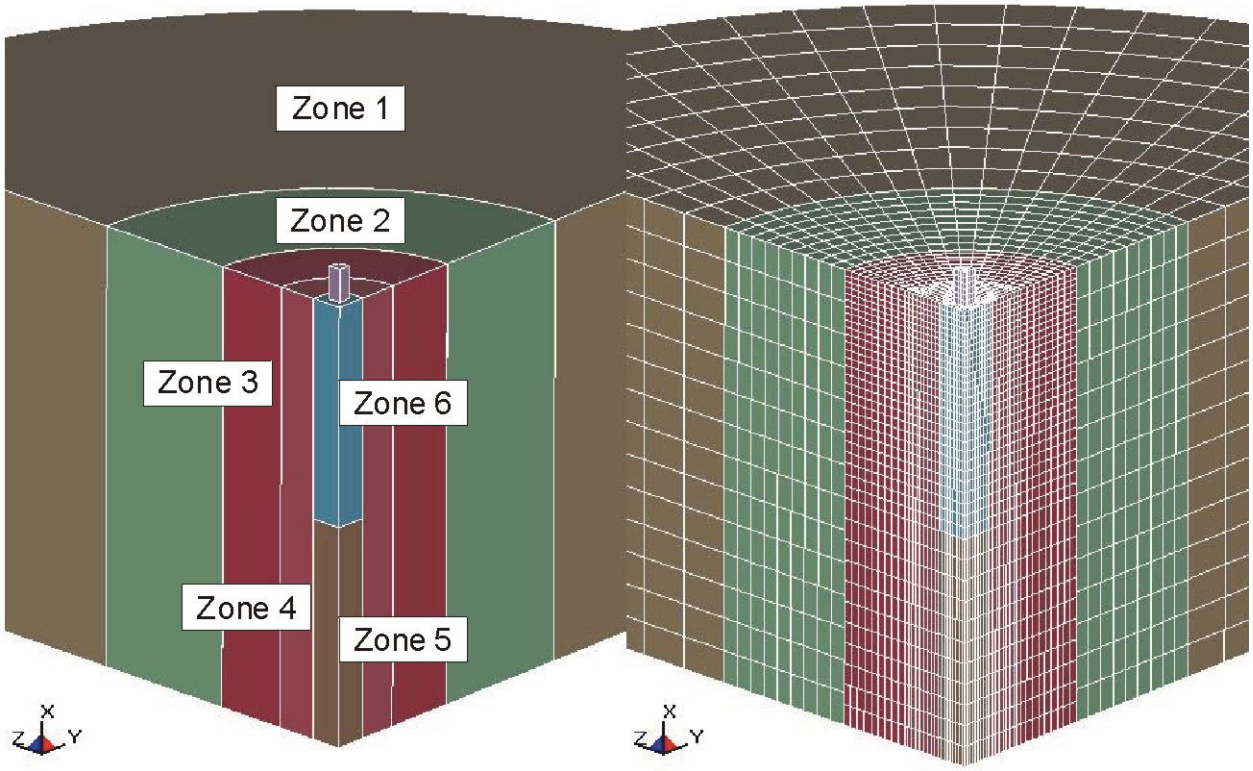

Figure 1 Quarter cylinder model (left) and corresponding mesh (right) used in the baseline Lagrange impact simulations.

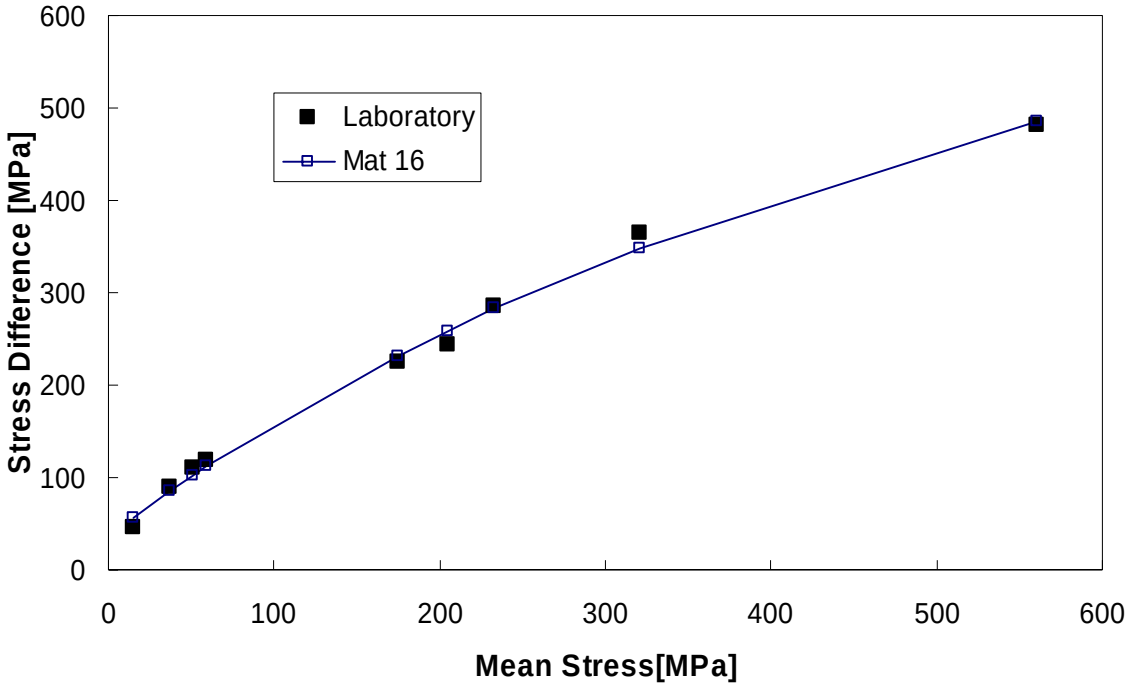

Figure 2 Shear failure surface for ERDC 46 MPa concrete.

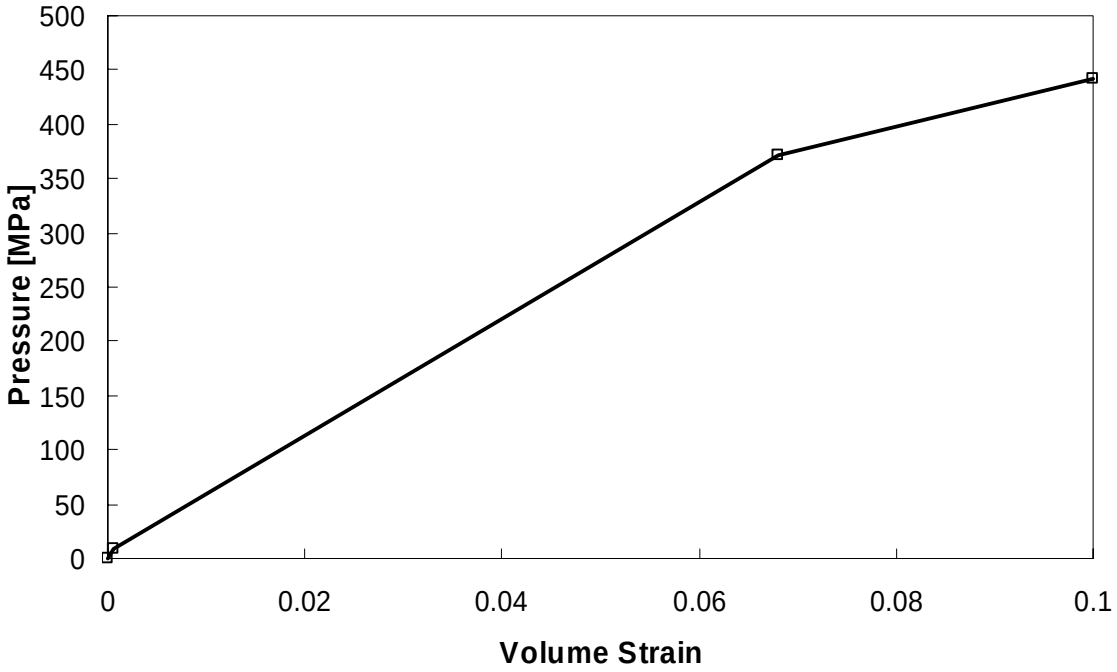

Figure 3 Pressure versus volume strain for ERDC 46 MPa concrete.

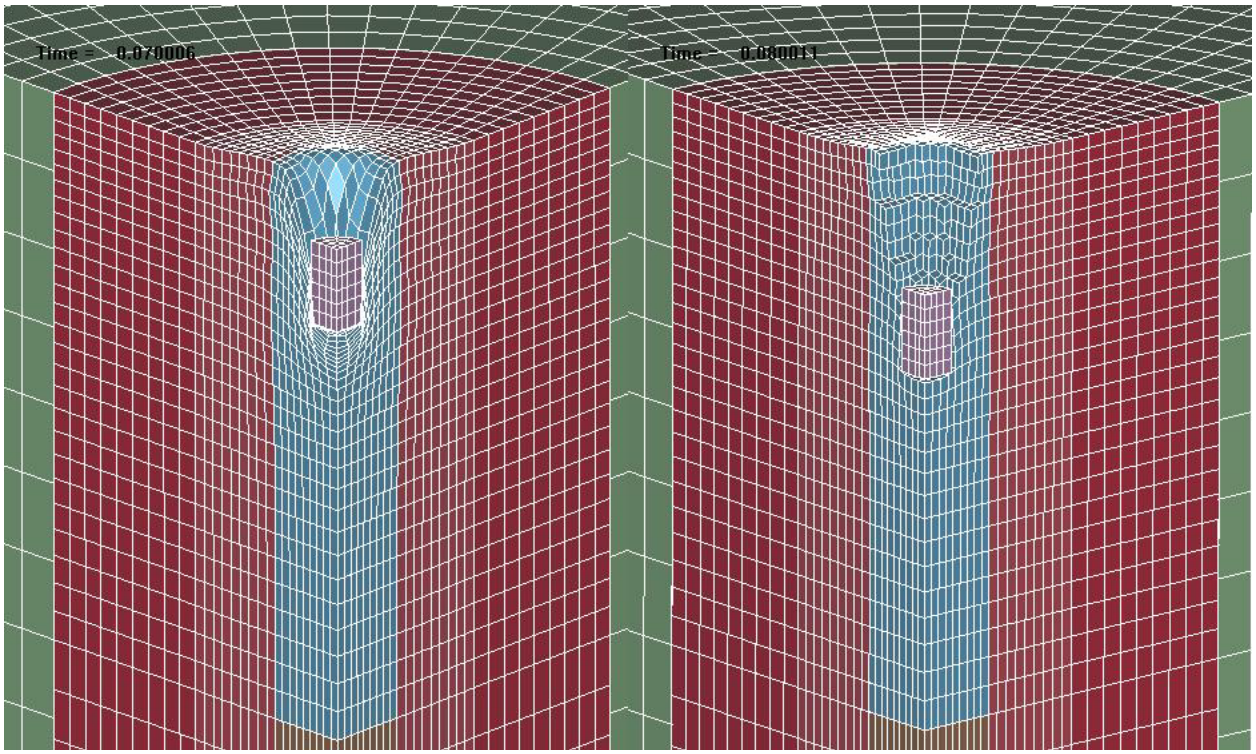

Figure 4 Lagrange impact simulations without (left) and with (right) element erosion.

Lagrange simulations

A baseline for assessing the performance of the analysis techniques is established by simulating the fragment impact using an all Lagrangian, i.e. 8 node solid elements with one point integration, simulation. Two Lagrange simulations were performed, without and with element erosion. The interface between the fragment and the target was an eroding surface-to-surface contact surface. This type of interface updates the definitions of the contact surfaces as elements are eroded.

The initial Lagrangian mesh was shown previously in Figure 1. The corresponding deformed final state mesh for the two Lagrange simulations are shown in Figure 4 for the no element erosion simulation (left), and with element erosion (right). It is something of a surprise that the simulation without erosion was able to run to completion. However, the average time step in the no erosion simulation was about an order-of-magnitude smaller, due to severe mesh distortions, than in the simulation with erosion.

LS-DYNA provides the user with several criteria for removing elements from a simulation. The criteria selected for the erosion simulation were a maximum principal strain of 25% (tension) or a minimum principal strain of -90% (compression); the criteria are implemented in a logical “or” fashion, i.e. the element is eroded if either criterion is exceeded. As mentioned previously, such erosion criteria are as hoc. For geomaterials, the use of principal strain criteria may be preferred over stress-based criteria since the material model provides an elastic-perfectly-plastic response, i.e. the stress state is already limited by the shear failure surface. Thus what remains unbounded, in the material model, is the amount of strain the material experiences at the limiting stress state. The particular values of principal strain used in this simulation were selected with a few

iterations to calibrate the depth of penetration to about 30 mm, and to illustrate the erosion analysis capability. No claim is made that these are the 'best,' or even *unique*, erosion criteria for this simulation.

Eulerian Simulation

The initial mesh for the Eulerian fragment impact simulation is essentially the same as the mesh used in the Lagrange simulations. The Eulerian mesh uses an additional layer of Eulerian elements above the impact region that is modeled as a vacuum; see left side of Figure 5. This region is provided to allow impact crater ejecta, i.e. concrete material, to flow (advect) out of the Eulerian concrete elements near the impacting fragment. This vacuum region simply provides an additional Eulerian domain definition for the purpose of monitoring ejecta. If ejecta was not of interest, the vacuum region could be omitted and the ejected material (momentum) would simply be advected out of the problem (domain). As mentioned previously, only the upper portion of the hexahedra region immediately under the fragment is modeled with Eulerian elements containing concrete, the remainder of the domain is modeled as Lagrange, i.e. 8 node solid elements.

The interface between the Eulerian concrete and the Lagrange rigid projectile is treated via a constraint formulation referred to as "Constrained Lagrange in Solid." This constraint formulation allows Lagrangian objects to move through an Eulerian mesh without mixing of the materials representing the Eulerian and Lagrange species. This interface specification requires the user to specify several contact type parameters, the most important of which are the parameters associated with the 'leakage' of Eulerian material into that portion of an Eulerian element that is occupied by the constrained Lagrange material. Note this does not indicate a 'fuzzy' boundary for the projectile, but rather a small region where the two materials may overlap. As in other penalty methods, the leakage can be minimized, but at the expense of a decreased stable time step.

A convenient feature of the LS-DYNA Eulerian implementation is that Eulerian elements may be connected directly to Lagrange elements, with the shared nodes being treated as Lagrange. The LS-DYNA Eulerian implementation first performs a purely Lagrange step, and then determines the amount of advection that must occur between adjacent elements to restore the mesh to its initial (Eulerian) configuration. So for shared nodes, there is no advection from the Eulerian to the Lagrange elements. The deformation of the Lagrangian mesh, in this Eulerian simulation, can be seen in the right half of Figure 5 near the top of the model along the shared Eulerian & Lagrangian region, i.e. Zones 4 & 6 shown previously in Figure 1.

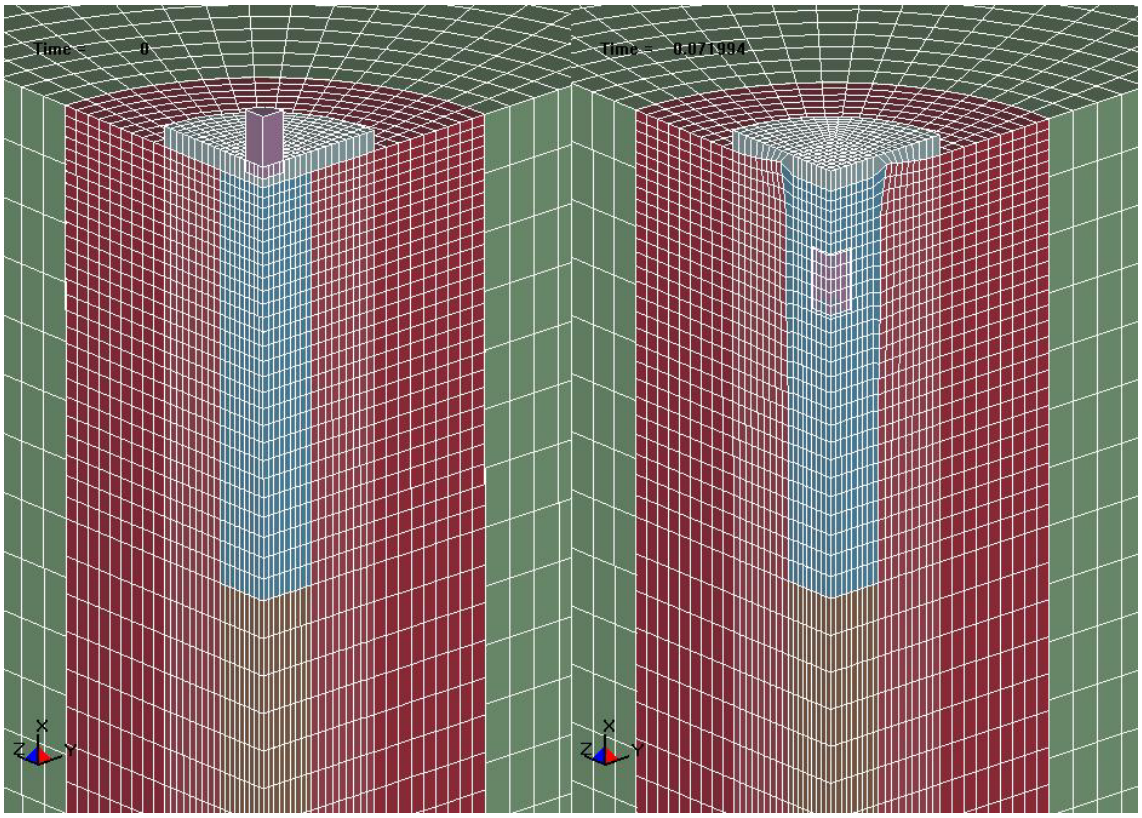

Figure 5 Initial Eulerian mesh (left) and at maximum fragment depth of penetration (right).

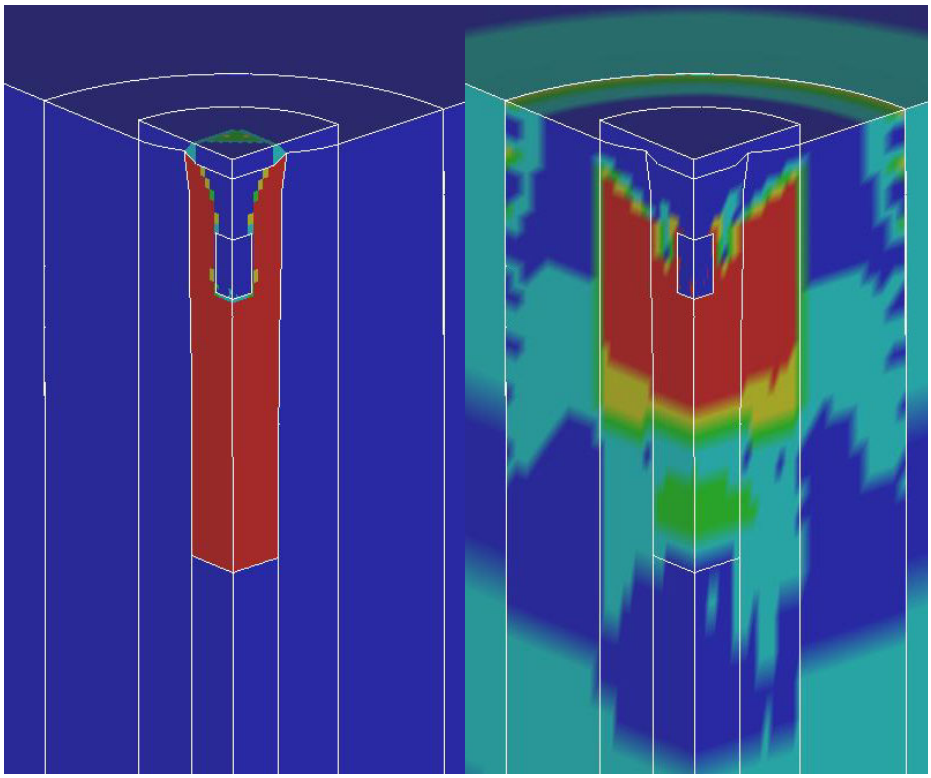

Figure 6 Fringes of volume fraction of concrete (left) and mean stress (right) at maximum fragment depth of penetration

Figure 6 shows the configuration for the Eulerian simulation at the time corresponding to the fragment's maximum depth of penetration into the concrete. The left side shows fringes of volume fraction of concrete in the Eulerian portion of the mesh, i.e. Zone 6 and the vacuum above. The red regions are concrete, with a volume fraction of one, and the blue regions are vacuum with a volume fraction of zero; the volume fraction is zero in all the Lagrange portion of the mesh by default. The right side of Figure 6 shows fringes of mean stress (pressure) at the same time. The mean stress fringes are at a fairly low level (-10 to 40 MPa) and serve to provide the reader with an indication of the degree of symmetry maintained in this simulation that combines Eulerian and Lagrangian formulations to represent the concrete, with the rigid fragment moving through the Eulerian portion of the mesh.

Smooth Particle Hydrodynamics (Meshfree) Simulation

The initial mesh for the Smooth Particle Hydrodynamics (SPH) fragment impact simulation replaces the upper hexahedra impact region of the baseline Lagrange mesh, with a collection of SPH particles; see Figure 7 (left). For the previously shown Eulerian and Lagrange simulations, the upper hexahedra fragment impact region was modeled using 2,187 elements (9x9x27) or 2,800 nodes. For the SPH simulation, this region was replaced by 9,216 SPH nodes (12x12x64) as it is recommended that additional SPH nodes be used to replace each 8-node solid Lagrange element, because of the interpolative basis used in the SPH formulation. Although not shown here, the mesh for the rigid fragment was also made more coarse for the SPH simulations, as the node-to-surface contact interface used between the SPH particles and the fragment's outer surface performs better when there are several SPH particles interacting with each segment of the Lagrange contacting body. Additionally, in the SPH region of the domain, two special SPH symmetry planes were defined. These symmetry planes internally define a set of 'ghost' particles to implement the symmetry constraint on the SPH particles nearest the symmetry planes. Finally, the SPH particle are connected to the remainder of the Lagrange mesh through the use of another constraint interface that ties the SPH particles to the corresponding surfaces of the Lagrange solid elements.

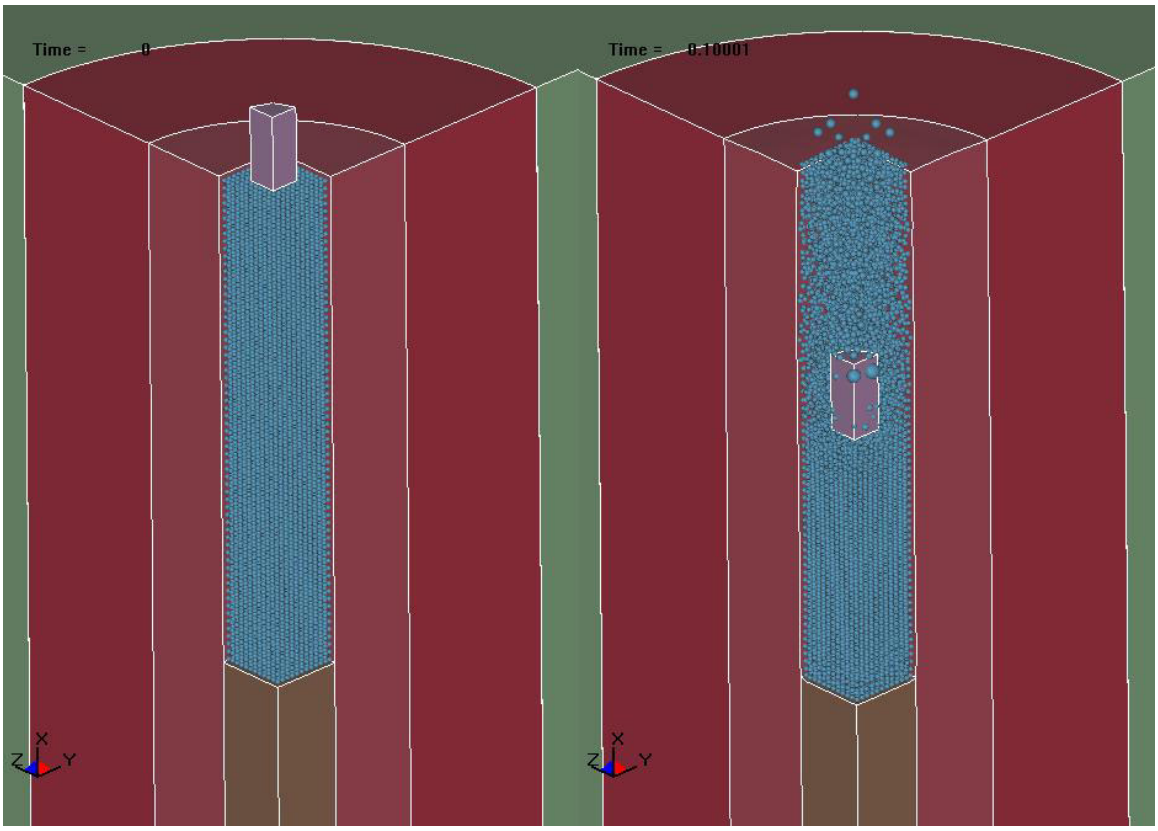

Figure 7 Initial SPH mesh (left) and final deformed configuration (right).

The right side of Figure 7 shows the final deformed SPH configuration for the fragment impact simulation. Some of the large SPH particles shown in this figure, especially the particles in front of the fragment, are a result of the graphical post-processor (LS-PrePost) increasing the diameter of the spheres, representing the SPH particles, when particle-to-particle spacing increases. As was done for the previously shown Eulerian simulation, Figure 8 shows fringes of low level (-10 to 40 MPa) mean stress to provided the reader with an indication of how well symmetry is preserved between the SPH and Lagrange portions of the mesh in this simulation.

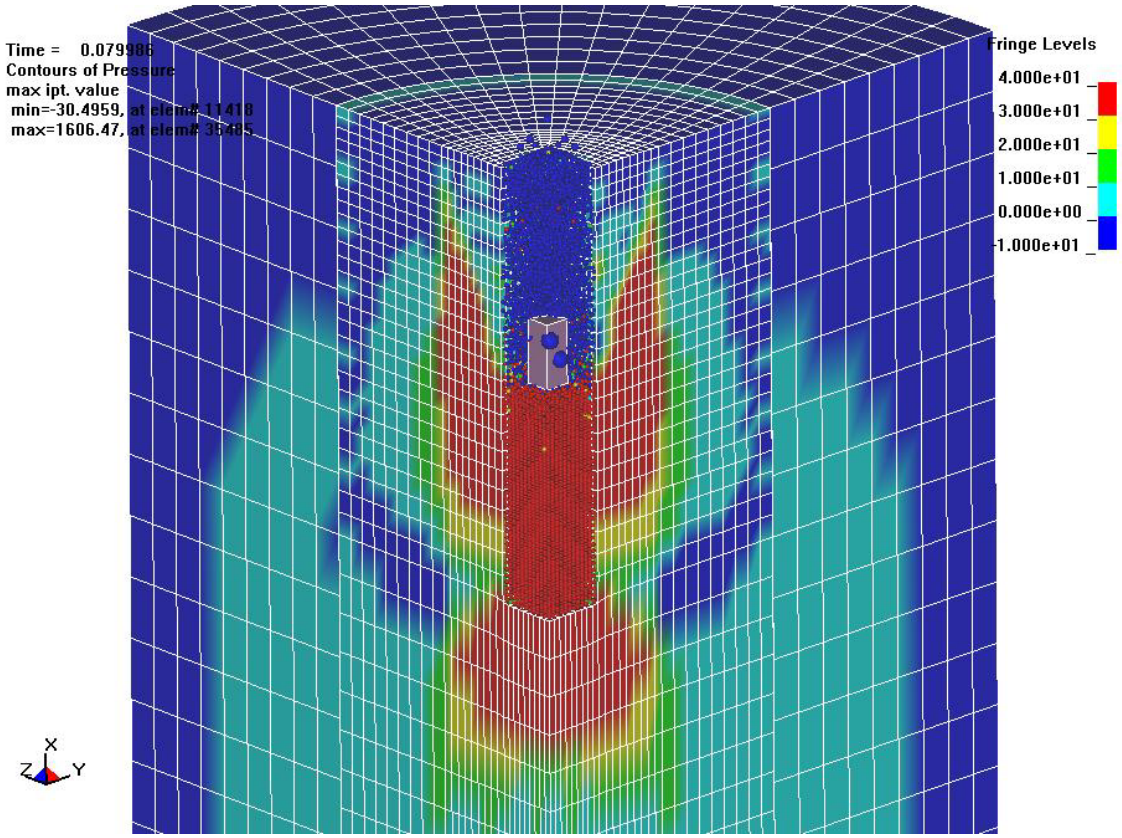

Figure 8 Fringes of mean stress (pressure) in the SPH particles and surrounding Lagrange mesh near the end of the simulation.

Comparison of Results

There are many aspects of these multi-formulation simulations that can be compared, and indeed need to be studied in detail to provide some degree of confidence that the results are correctly representing the physics. For the purposes of this preliminary assessment, the velocity history of the fragment is chosen as the metric for the comparison of the results. Recall the fragment's initial speed is 1068 mm/msec and a realistic estimate of the fragment penetration into the target is about 30 mm from the impact surface. As discussed below, the fragment velocity histories provide some insight into how well the various analysis formulations compare for this simulation. The calculated depth of penetration is only used as a calibration point.

Figure 9 shows a comparison of the fragment velocity histories for the four impact simulations reported. Recall the principal strains, used in the Lagrange simulation with erosion, were *calibrated* to provide 30 mm of fragment displacement. As noted previously, the Lagrange simulation without erosion predicted less depth of penetration for the fragment (21 mm), and thus its velocity history passes through the point of zero velocity before the correspond Lagrangian simulation curve with erosion; the small positive final velocity of the fragment indicates it is rebounding away from the crater in the concrete slab.

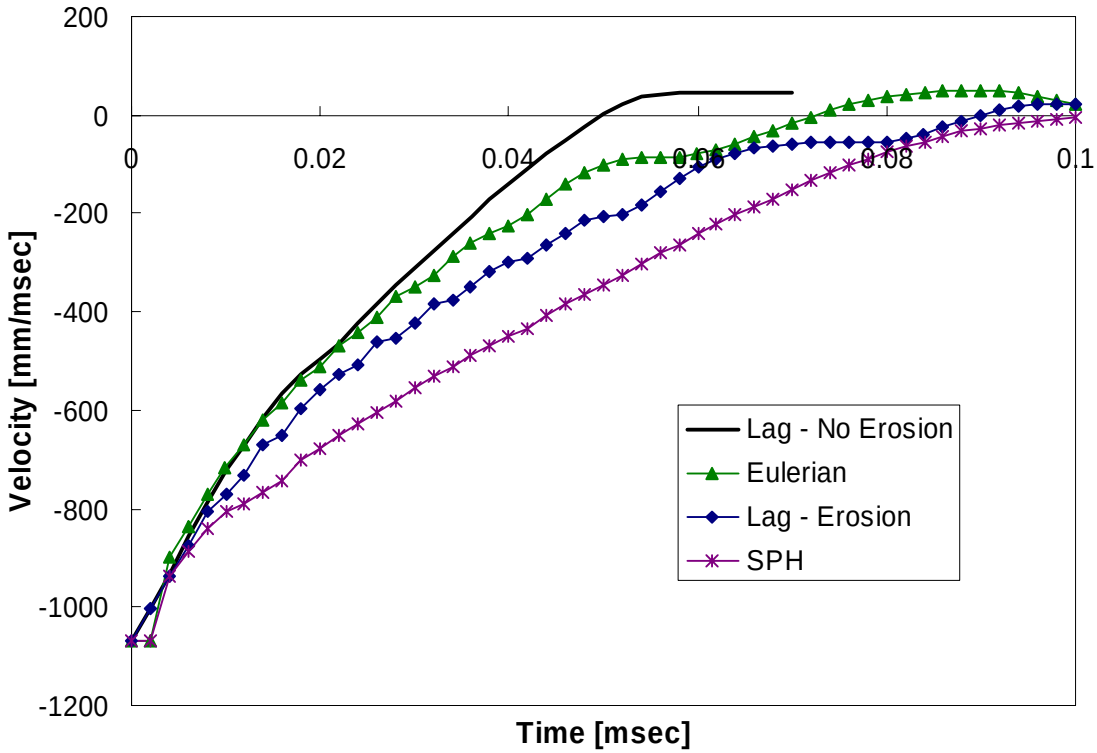

Figure 9 Velocity histories of the rigid fragment for four impact simulations.

The velocity history for the Eulerian simulation follows the corresponding velocity history of Lagrange-without-erosion simulation for about the first 0.028 milliseconds. The Eulerian velocity history then deviates from the Lagrange-without-erosion simulation and lies between the two Lagrange simulations, with a maximum depth of penetration of 25 mm, compared to the 21 mm for the Lagrange simulation without erosion, and 30 mm for the calibrated Lagrange simulation with erosion.

The very early time portion of the Eulerian velocity history indicates no change in the velocity. From time zero to about 0.002 milliseconds, there is no decrease in the velocity of the fragment, indicating that the Eulerian concrete material is not interacting with the fragment. Recall that during the initial portion of the impact simulation the incremental strain-rates are quite large, this fact, combined with this observed lack of coupling between the Eulerian concrete and Lagrange rigid fragment, may indicate that a smaller time increment is needed initially to improve this coupling and minimize the aforementioned leakage that can occur in such coupled Eulerian and Lagrangian simulations.

The velocity history for the SPH simulation also seems to have an early time problem coupling with the rigid Lagrange fragment, however the SPH velocity history then tracks the velocity histories of the other three simulations, i.e. both the Lagrange and the Eulerian simulations, until about 0.01 milliseconds. After this time the SPH velocity history indicates the concrete material provides less resistance to penetration than in the other simulations; the final depth of penetration is 38.6 mm which is greater than that calculated in any of the other formulations. No explanation

for this behavior of the SPH simulation is offered, however the infamous 'tensile instability' of SPH methods is always a possible culprit.

Conclusions

As demonstrated in the present work, the Eulerian and Smooth Particle Hydrodynamics (meshfree) methods offer the analyst interested in simulating penetration and perforation an alternative to performing a Lagrange simulation with ad hoc erosion criteria. However, the attractiveness of these alternate analysis formulations needs to be tempered with the knowledge that the prospective user will need to devote a considerable amount of effort to becoming proficient in their application.

Obviously there is a lot more to be learned about the application of the Eulerian and SPH techniques to penetration and perforation, and hopefully much more to be gained from the effort. The present plan is to master the SPH technique as there is interest in applying the technique to other applications where catastrophic material and structural failure are dominate. A parallel path of improving the modeling of the dynamic and tensile response of concrete is also planned. The hope is the combination of a more robust analytical technique, i.e. SPH, and a more realistic constitutive model will provide credible simulations of impact, penetration, perforation, and failure of concrete structures.

Acknowledgements

The author is grateful to Drs. Jean Luc Lacome, and M'hamed Souli, of Livermore Software Technology Corporation (LSTC) for many useful discussions related to application of the LS-DYNA SPH, and Eulerian, capabilities, respectively. Thanks also to Dr. Steve Attaway of Sandia National Laboratories for suggesting a refinement in the SPH particle grid that dramatically improved the results.

References

[J.O. Hallquist, "LS-DYNA Keyword User's Manual", Version 970, Livermore Software and Technology Corporation, Livermore CA, April 2003.